Article

Cell Reports

Loss of the Otx2-Binding Site in the Nanog Promoter Affects the Integrity of Embryonic Stem Cell Subtypes and Specification of Inner Cell Mass-Derived Epiblast

Graphical Abstract

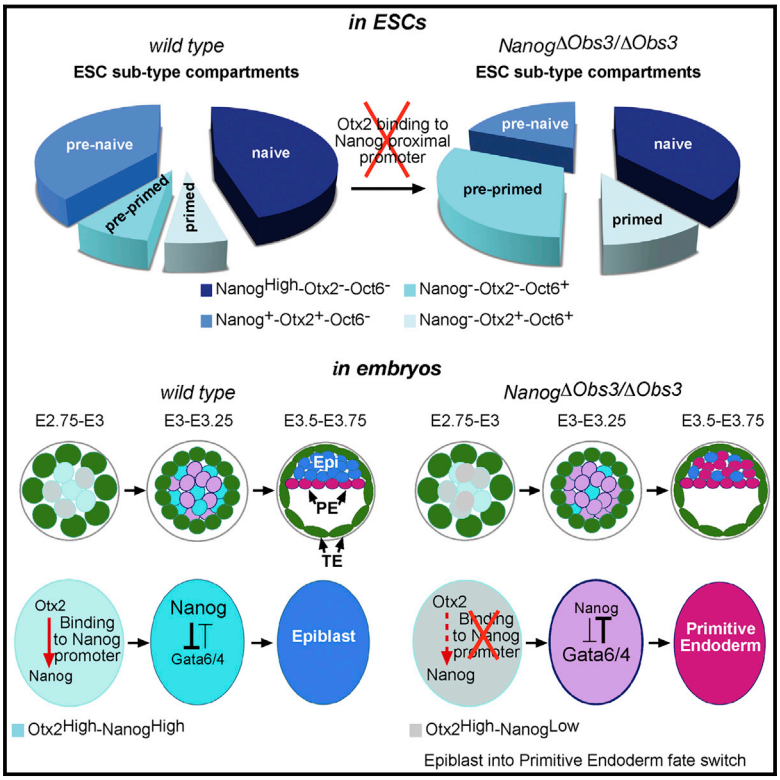

Highlights

- Otx2 binds to the promoter/enhancer region of Oct4, Sox2, and Nanog in ESCs and EpiSCs
- Otx2 binding to the Nanog promoter helps maintain the integrity of ESC compartments
- Loss of this Otx2-binding site induces primed-like features in ESCs
- Otx2 regulation of Nanog contributes to ICM differentiation of the epiblast

Authors

Dario Acampora, Daniela Omodei, Giuseppe Petrosino, ..., Luca Giovanni Di Giovannantonio, Vincenzo Mercadante, Antonio Simeone

Correspondence

antonio.simeone@igb.cnr.it

In Brief

Acampora et al. find that loss of the Otx2-binding site in the Nanog promoter affects the size of specific ESC-subtype compartments and differentiation of the ICM-derived epiblast lineage. This regulation contributes to maintaining the integrity of the ESC state and to specifying the epiblast cell lineage during preimplantation development.

Accession Numbers

E-MTAB-3856

Acampora et al., 2016, Cell Reports *15*, 2651–2664
June 21, 2016
http://dx.doi.org/10.1016/j.celrep.2016.05.041

Cell Reports
Article

Loss of the Otx2-Binding Site in the Nanog Promoter Affects the Integrity of Embryonic Stem Cell Subtypes and Specification of Inner Cell Mass-Derived Epiblast

Dario Acampora,[1,2] Daniela Omodei,[1] Giuseppe Petrosino,[3] Arcomaria Garofalo,[4,5] Marco Savarese,[4,5] Vincenzo Nigro,[4,5] Luca Giovanni Di Giovannantonio,[1] Vincenzo Mercadante,[1] and Antonio Simeone[1,2,*]
[1]Institute of Genetics and Biophysics "Adriano Buzzati-Traverso," CNR, Via P. Castellino 111, 80131 Naples, Italy
[2]IRCCS Neuromed, 86077 Pozzilli (IS), Italy
[3]Dipartimento di Medicina Molecolare e Biotecnologie Mediche, Università degli Studi di Napoli Federico II, Via Sergio Pansini 5, 80131 Naples, Italy
[4]Dipartimento di Biochimica, Biofisica e Patologia Generale, Seconda Università degli Studi di Napoli, Via L. De Crecchio, 7, 80138 Naples, Italy
[5]Telethon Institute of Genetics and Medicine (TIGEM), Via Campi Flegrei, 34, 80087 Pozzuoli (NA), Italy
*Correspondence: antonio.simeone@igb.cnr.it
http://dx.doi.org/10.1016/j.celrep.2016.05.041

SUMMARY

Mouse embryonic stem cells (ESCs) and the inner cell mass (ICM)-derived epiblast exhibit naive pluripotency. ESC-derived epiblast stem cells (EpiSCs) and the postimplantation epiblast exhibit primed pluripotency. Although core pluripotency factors are well-characterized, additional regulators, including Otx2, recently have been shown to function during the transition from naive to primed pluripotency. Here we uncover a role for Otx2 in the control of the naive pluripotent state. We analyzed Otx2-binding activity in ESCs and EpiSCs and identified Nanog, Oct4, and Sox2 as direct targets. To unravel the Otx2 transcriptional network, we targeted the strongest Otx2-binding site in the Nanog promoter, finding that this site modulates the size of specific ESC-subtype compartments in cultured cells and promotes Nanog expression in vivo, predisposing ICM differentiation to epiblast. Otx2-mediated Nanog regulation thus contributes to the integrity of the ESC state and cell lineage specification in preimplantation development.

INTRODUCTION

In mammals, the progenitors of extraembryonic and embryonic tissues are established during preimplantation development (Hermitte and Chazaud, 2014; Martinez Arias et al., 2013; Schrode et al., 2014; Ohnishi et al., 2014). Differentiation of the first extraembryonic cell lineage occurs at late morula stage and generates the trophectoderm (TE) and inner cell mass (ICM), which in turn differentiate into a second extraembryonic tissue, the primitive endoderm (prE), and the epiblast from which all embryonic and adult tissues are generated. Mouse embryonic stem cells (ESCs) are derived from the ICM and early preimplantation epiblast (Evans and Kaufman, 1981; Martin, 1981; Rossant, 2008; Silva and Smith, 2008; Silva et al., 2009; Nichols and Smith, 2009; Hanna et al., 2010; Boroviak et al., 2014). ESCs may efficiently integrate into host blastocysts and differentiate into all embryonic cell lineages, and their state depends on a self-maintaining network controlled by core pluripotency factors Oct4 (also known as Pou5f1), Nanog, Sox2, Klf2/4, and Esrrb, as well as the LIF-, WNT-, and BMP4-signaling pathways. Indeed, these factors together define a dynamic mechanism that ensures indefinite self-renewal and protects ESCs from lineage commitment (Chambers et al., 2007; Niwa et al., 2009; Hanna et al., 2010; Lanner and Rossant, 2010; Zhang et al., 2010; Lyashenko et al., 2011; ten Berge et al., 2011; Festuccia et al., 2012).

ESCs grown in serum plus LIF exhibit cell-to-cell reversible differences in the expression level and sensitivity to specific transcription factors (TFs) and signaling molecules, which together maintain the balance between high self-renewal and susceptibility to differentiation (Hayashi et al., 2008; Silva and Smith, 2008; Ying et al., 2008; Toyooka et al., 2008; Kalmar et al., 2009; Nichols and Smith, 2011; Smith, 2013; Torres-Padilla and Chambers, 2014). However, when cultured in the presence of LIF and two inhibitor molecules (2i), which block glycogen synthase kinase3 (GSK3) and mitogen-activated protein kinase MEK, ESCs exhibit homogeneous expression of naive pluripotency TFs and striking similarity to the preimplantation epiblast (Ying et al., 2008; Nichols and Smith, 2009; Nichols et al., 2009; Silva et al., 2009; Osorno and Chambers, 2011; ten Berge et al., 2011; Marks et al., 2012; Boroviak et al., 2014).

Mouse epiblast stem cells (EpiSCs) have been classically derived from the epiblast of postimplantation pre-grastrula embryos and express Oct4, Sox2, and a low level of Nanog together with Fgf5, brachyury (T), and other specific markers. EpiSCs cannot generate chimeric embryos when injected into host blastocysts, and their self-renewal and undifferentiated state depend on FGF and activin A pathways (Brons et al., 2007; Tesar et al., 2007; Hanna et al., 2010; Zhang et al., 2010; Lanner and Rossant, 2010; Kunath, 2011; Najm et al., 2011; Greber et al., 2010). The homeodomain TF Otx2 is expressed in both ESCs and EpiSCs

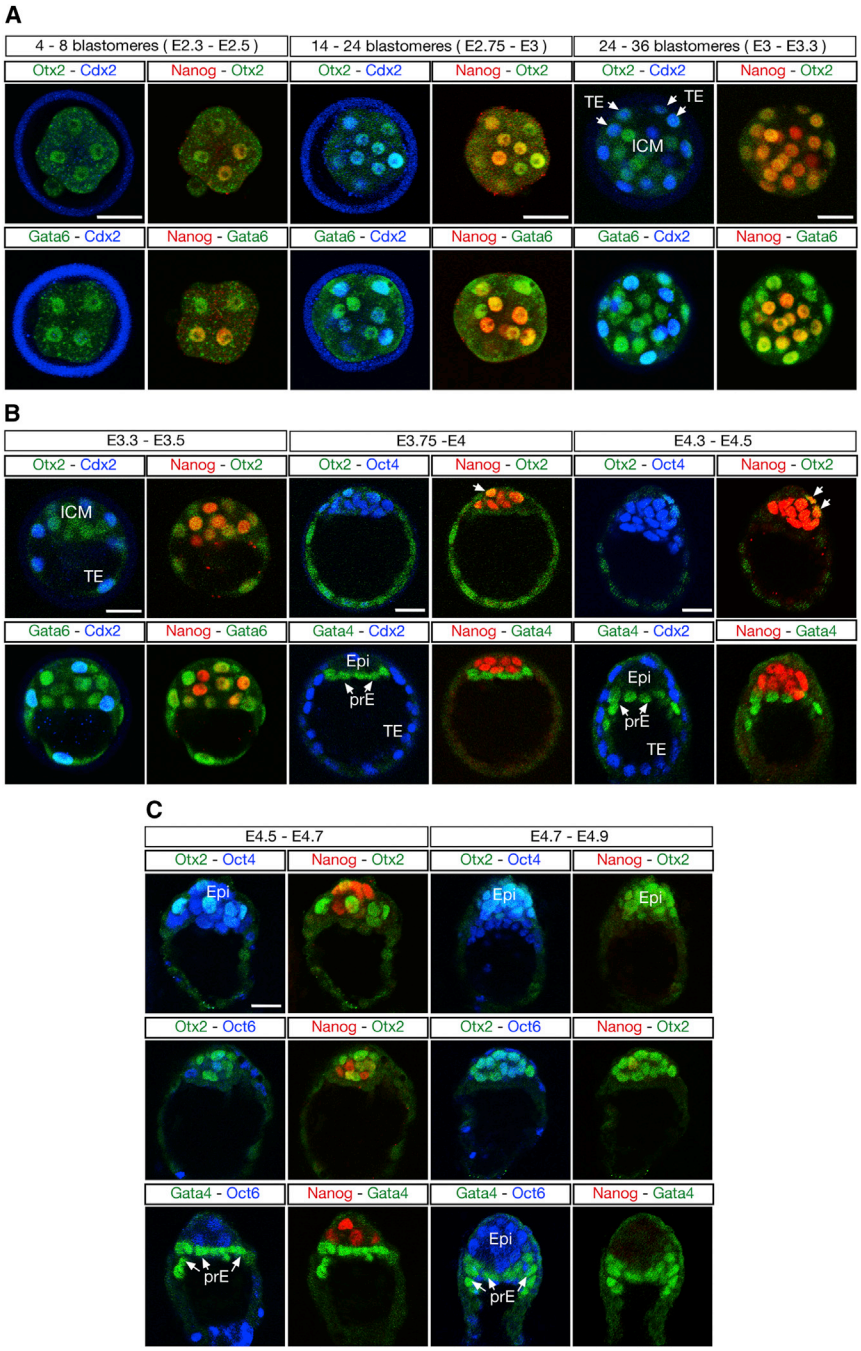

Figure 1. Otx2 Expression in Preimplantation Mouse Embryos

(A) Immunostaining with Otx2, Nanog, and Cdx2 and with Gata6, Nanog, and Cdx2 was performed at early morula (8 blastomeres), mid-morula (14–24 blastomeres), and late morula (24–36 blastomeres).

(B) Immunostaining with Otx2, Nanog, and Cdx2; with Gata6, Nanog, and Cdx2; with Otx2, Nanog, and Oct4; and with Gata4, Nanog, and Cdx2 was performed at E3.3–E3.5, E3.75–E4, and E4.3–E4.5 to follow Otx2 expression during ICM differentiation into prE (Gata4/6^{+}) and epiblast (Nanog^{+}). In this context Oct4 is detected in both ICM derivatives and Cdx2 in TE; note that Otx2 is attenuated in the ICM at E3.3–E3.5, and, between E3.75 and E4.5, it is detected sporadically in the epiblast (arrows).

(C) Immunostaining with Otx2, Nanog, and Oct4; with Otx2, Nanog, and Oct6; and with Gata4, Nanog, and Oct6 shows that, at E4.5–E4.7, Nanog is detected in about 50% of epiblast cells and, at E4.7–E4.9, only in a few epiblast cells and at a low level. Conversely, Otx2 is strongly upregulated and at E4.7–E4.9 it is co-expressed with Oct6 in all epiblast cells. Epi, epiblast; prE, primitive endoderm; TE, trophectoderm; ICM, inner cell mass. Scale bars, 30 μm.

as well as in preimplantation and postimplantation embryos (Acampora et al., 2013). Previous studies have indicated that Otx2 is required (1) in ESCs cultured in serum with LIF to antagonize naive pluripotency (Acampora et al., 2013), (2) in EpiSCs to stabilize their state by suppressing mesendoderm into neural fate switch (Acampora et al., 2013), and, more recently, (3) for transition of naive into primed pluripotency by recruiting Oct4 at new enhancers associated to ESC-derived epiblast-like cell (EpiLC) differentiation (Buecker et al., 2014; Yang et al., 2014). Here we have investigated the functional relevance of the transcriptional network controlled by Otx2 in ESCs, EpiSCs, and in vivo. We show that loss of the Otx2-binding site in the Nanog promoter affects, in LIF/FBS growth conditions, the integrity of specific ESC-subtype compartments and, in vivo, impairs the differentiation of the ICM into the epiblast lineage.

RESULTS

Otx2 Expression in Preimplantation Development

First we analyzed the Otx2 expression during preimplantation development in comparison with that of markers specific for TE and ICM derivatives corresponding to Cdx2 (TE), Gata6 (early prE), Gata4 (late prE), and Nanog (epiblast) (Frankenberg et al., 2011; Grabarek et al., 2012; Martinez Arias et al., 2013; Hermitte and Chazaud, 2014). At early morula (four to eight blastomeres), Otx2 was detected at a low level, while at mid-morula (14–24 blastomeres) its expression level was increased and its distribution shared with Gata6, Nanog, and Cdx2 (Figure 1A). Between embryonic day (E)3.0 (24–36 blastomeres) and E3.5, Otx2 expression was higher in most of the ICM cells co-expressing Nanog and Gata6 (Figures 1A and 1B), from E3.5 up to E4.5 Otx2 was gradually downregulated in the ICM, and from E3.75 up to E4.5 it was almost completely excluded from epiblast and expressed at a low level in TE (Figure 1B). Between E4.5 and E5.0, Nanog

expression gradually declined, and at E4.7–E4.9 it was almost undetectable (Figure 1C); in contrast, Otx2 was strongly re-activated, first in epiblast cells expressing a low level of Nanog and then in all epiblast cells (Figure 1C).

Interestingly, we found that also Oct6, a marker specific for primed epiblast (Buecker et al., 2014), was activated between E4.5 and E4.9 in Nanog^{-} or Nanog^{-}-Otx2^{+} epiblast cells (Figure 1C). Thus, the expression code detected in the epiblast between E3.75 and E4.5 (Otx2^{-}-Oct6^{-}-Nanog^{+}) mirrors that observed at E4.7–E4.9 (Otx2^{+}-Oct6^{+}-Nanog^{-}), strongly suggesting that full activation of Otx2 and Oct6 in the epiblast defines the onset of early primed pluripotency before embryo implantation. This also is supported by overt similarity in Otx2, Oct6, and Nanog expression profiles between late preimplantation and early postimplantation epiblasts (see below). Therefore, these data suggest that Otx2 may play a role in vivo for initiating the naive-to-primed transition and, in addition, that Otx2 may have a distinct role at early ICM differentiation stage supporting the naive TF network.

Identification of Otx2-Binding Sites in ESCs and EpiSCs

Based on previous data (Figure 1) (Acampora et al., 2013; Buecker et al., 2014; Yang et al., 2014), we investigated the Otx2 transcriptional network by chromatin immunoprecipitation sequencing (ChIP-seq) experiments in wild-type (WT) ESCs and day 4 (d4) EpiSCs, using as negative control ESCs and EpiSCs lacking Otx2. Total Otx2 peaks and associated genes are shown (Table S1). In this study, we focused on Otx2 peaks detected within a 10-kb genomic region located upstream of the transcription start site (TSS) of the closest gene. We identified 4,886 putative Otx2 target genes in EpiSCs and 874 in ESCs; 611 of these were shared by ESCs and EpiSCs (Figure 2A; Table S2). Then we analyzed the Otx2 peaks identified upstream of the 611 genes, and we found that 508 peaks were retained in both ESCs and EpiSCs, 690 were enhanced in EpiSCs, and 225 were enhanced in ESCs (Figure 2B; Table S3). Importantly, numerous genes involved in pluripotency network control were identified as Otx2 targets, and among these were *Oct4*, *Nanog*, and *Sox2* (Table S4). To validate Otx2 binding to *Nanog*, *Oct4*, and *Sox2*, we analyzed the genome browser representation of ChIP-seq profiles and focused the validation assays on the regions covered by Otx2 peaks (pink area in Figures 2C–2E). Sequence analysis of the genomic region including the Otx2 peaks showed that they contain one or more Otx2 recognition sequences (Orss) (GGATTA) (Figures 2F–2H) (Buecker et al., 2014). All ChIP peaks were validated in ESCs and/or EpiSCs (Figures 2I and 2J), thus indicating that Otx2 may bind the promoter/enhancer region of core pluripotency factors in both pluripotent stem cells. Notably, compared to EpiSCs, the diminished Otx2-binding efficiency detected in ESCs may be partly due to the reduced percentage of ESCs expressing a high level of Otx2 or to a decreased Otx2 binding affinity.

Loss of the Otx2-Binding Site 3 in the Nanog Promoter Region Affects the Integrity of ESC Compartments

To examine the hypothesis that Otx2 may play a role in support of the naive pluripotency network, we generated an ESC line carrying the selective mutagenesis (GGGATTAA into CGACAGTT) of the Otx2-binding site 3 (Obs3), which was located 144 bp upstream of the *Nanog* TSS and showed the highest Otx2-binding enrichment when compared to Obs1 and Obs2 in ChIP assays (Figures 2I, 2J, and S1A–S1D). First, we analyzed in *Nanog*$^{\Delta Obs3/+}$ heterozygous ESCs, which exhibited a WT-like phenotype, whether Otx2 binding to Obs3 was affected by the Obs3 mutagenesis. To this aim we performed allele-specific ChIP assays showing selective abrogation of Otx2 binding to the mutagenized Obs3 (Figure S1E). Conversely, the binding of Oct4, whose recognition sequence (Oct4bs) is located 36 bp upstream of Obs3, appeared similar on both WT and Obs3-mutated alleles (Figure S1E). Otx2 binding to the mutagenized Obs3 was abolished in *Nanog*$^{\Delta Obs3/\Delta Obs3}$ mutant ESCs and EpiSCs, whereas binding to Obs1 and Obs2 was unaffected (Figure 3A). Compared to WT, *Nanog*$^{\Delta Obs3/\Delta Obs3}$ ESCs showed flat morphology and a marked reduction in the number of colonies uniformly stained with alkaline phosphatase (ALP) (45 ± 13 versus 231 ± 26 of WT) (Figure 3B).

A detailed analysis was performed to assess whether loss of Obs3 affects the identity and size of ESC-subtype compartments. Previous studies have indicated molecular markers and functional features specific for naive and primed cells (Toyooka et al., 2008; Silva et al., 2009; Hanna et al., 2010; Lanner and Rossant, 2010; Marks et al., 2012; Acampora et al., 2013; Martinez Arias et al., 2013; Buecker et al., 2014; Torres-Padilla and Chambers, 2014; Kalkan and Smith, 2014). Based on these studies, we investigated the identity of Obs3 ESC subtypes by analyzing the combinatorial expression of four markers: Nanog, Otx2, Oct4, and Oct6. In these experiments, we referred to cells expressing Nanog, regardless of the protein level, as Nanog^{+} and to cells expressing a high or low level of Nanog as Nanog^{H} or Nanog^{L}, respectively. Cell counting analysis was performed on cytospun ESCs. Preliminary immunostaining assays performed with Otx2 and Oct6 and with Oct6 and Nanog showed that, compared to WT, mutant ESCs exhibited an increased number of Oct6^{+} cells and a reduction of those Otx2^{+} and Nanog^{+} (Figures 3E and S2A). Importantly, we found that Oct6^{+} cells were complementary to Nanog^{+} cells both in WT and Obs3 ESCs (Figures 3E and S2A).

We next assessed whether the size of ESC-subtype compartments was affected in Obs3 ESCs by counting ESCs after immunostaining with Oct4, Oct6, Nanog, and Otx2 (Figure S2). Compared to WT, the percentage of Oct4^{+} cells in Obs3 ESCs was substantially unaffected, although an increase in the proportion of Oct4^{L} cells was observed (33 ± 5 versus 14 ± 2 of WT) (Figures 3C, 3E, and S2A; Table S5). Analysis of Oct6 expression indicated that the Oct6^{+} subtype was greatly expanded in Obs3 ESCs (43 ± 7 versus 17 ± 3 of WT) (Figures 3C, 3E, and S2A; Table S5), preferentially in Oct4^{L} cells (Figures 3E and S2A). Analysis of Nanog and Otx2 co-immunostaining showed that, compared to WT, the percentage of total cells expressing Nanog was significantly reduced in Obs3 ESCs (47 ± 5 versus 79 ± 8 of WT). In particular, Nanog^{H} cells (36 ± 5 versus 52 ± 5 of WT) were diminished less severely than Nanog^{L} cells (10 ± 3 versus 26 ± 3 of WT) (Figures 3C and S2A; Table S5). Similarly, the percentage of cells expressing Otx2 was significantly reduced in Obs3 ESCs (28 ± 5 versus 45 ± 5 of WT) (Figures 3C and S2A; Table S5).

Next, to unambiguously assign the size and identity of ESC-subtype compartments, triple immunostaining for Otx2, Nanog, and

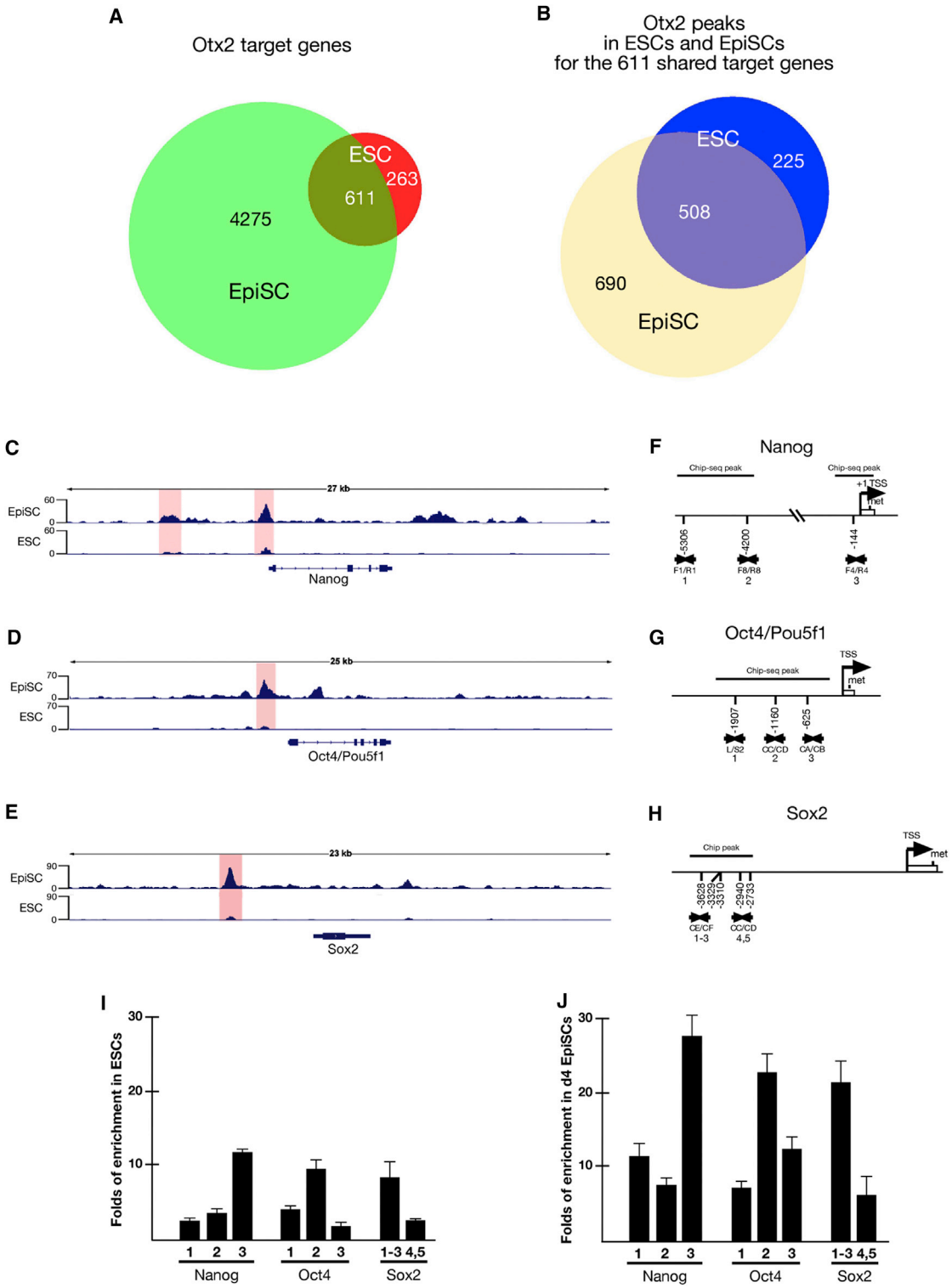

Figure 2. Otx2-Binding Activity in ESCs and EpiSCs Implies Direct Control of *Oct4*, *Nanog*, and *Sox2*

(A) Venn diagram shows the number of genes with Otx2 peaks located within 10 kb upstream of the TSSs in ESCs (red), EpiSCs (green), and in both cell lines (mustard).

(B) Venn diagram shows the distribution of peaks identified in 611 genes bound by Otx2 in both ESCs (blue) and EpiSCs (yellow); in particular, 508 of these peaks are shared by ESCs and EpiSCs, 690 are specific for EpiSCs, and 225 are specific for ESCs.

(legend continued on next page)

Oct6 was performed. Since the Otx2$^+$ subtype may co-express Nanog or Oct6, we first determined the size of the Otx2$^+$-Oct6$^-$ subtype compartment independently of Nanog expression, and we found that the number of Otx2$^+$-Oct6$^-$ cells was remarkably diminished in Obs3 ESCs (18 ± 3 versus 40 ± 5 of WT) (Figures 3D, 3E, and S2B; Table S5). We next analyzed the Oct6$^-$ subtypes and found that, compared to WT, in Obs3 ESCs they were all decreased as a percentage of the total cell number (36 ± 4 versus 48 ± 5 of WT for Nanog$^+$-Otx2$^-$-Oct6$^-$, 13 ± 2 versus 31 ± 4 of WT for Nanog$^+$-Otx2$^+$-Oct6$^-$, and 5 ± 1 versus 9 ± 1 of WT for Nanog$^-$-Otx2$^+$-Oct6$^-$) (Figures 3D, 3E, and S2B; Table S5). Notably, within the Nanog$^+$-Otx2$^-$-Oct6$^-$ cells, those exhibiting Nanog^H (Nanog^H-Otx2$^-$-Oct6$^-$) represented the large majority in both WT and Obs3 ESCs (33 ± 4 versus 45 ± 4 of WT) (Figures 3D and S2B; Table S5). Consistent with these findings, Oct6$^+$ ESC subtypes were increased in Obs3 ESCs (29 ± 4 versus 9 ± 1 of WT for Nanog$^-$-Otx2$^-$-Oct6$^+$ and 11 ± 2 versus 7 ± 2 of WT for Nanog$^-$-Otx2$^+$-Oct6$^+$) (Figures 3D and S2B; Table S5).

These findings indicate that, through the combined expression of Nanog, Otx2, Oct6, and Oct4, we identified in WT ESCs three major Oct4$^+$ compartments (Figure 3F). The first was Nanog$^+$ (Nanog$^+$-Otx2$^-$-Oct6$^-$), which accounted for about 48% of total ESCs and prevalently expressed Nanog^H. The second was Oct6$^+$, which accounted for 16% of total ESCs and included the Nanog$^-$-Otx2$^+$-Oct6$^+$ and the Nanog$^-$-Otx2$^-$-Oct6$^+$ sub-compartments. The third consisted of Otx2$^+$-Oct6$^-$ ESCs, which accounted for about 40% of total ESCs and included a large Nanog$^+$-Otx2$^+$-Oct6$^-$ sub-compartment and a small Nanog$^-$-Otx2$^+$-Oct6$^-$ sub-compartment (Figure 3F). We assigned the Nanog^H-Otx2$^-$-Oct6$^-$-Oct4$^+$ and the Nanog$^-$-Otx2$^+$-Oct6$^+$-Oct4$^+$ expression codes to cells, respectively, with naive-like and primed-like identities. Between these two extremes, we made the assumption that the Nanog$^-$-Otx2$^-$-Oct6$^+$-Oct4$^+$ and the Nanog$^+$-Otx2$^+$-Oct6$^-$-Oct4$^+$ expression profiles corresponded to transitional subtypes, respectively, close to the identity of primed-like and naive-like subtypes, which we called pre-primed-like and pre-naive-like. In this context, the Nanog$^-$-Otx2$^+$-Oct6$^-$-Oct4$^+$ small sub-compartment might represent an extension of the pre-naive-like sub-compartment (Figure 3F). Based on this identity code and compared to WT, in Obs3 ESCs the pre-naive-like and pre-primed-like sub-compartments were remarkably affected and their sizes even inverted; the primed-like sub-compartment was slightly expanded, and the naive-like sub-compartment was moderately but significantly reduced (Figure 3F). Importantly, in the pre-naive-like sub-compartment of WT ESCs, the expression levels of Nanog and Otx2 were not homogenous and most of the cells exhibited complementary expression levels (e.g., cells with a high or low level of Otx2 showed, respectively, a low or high level of Nanog) (Figure 3G). We suggest that, in Otx2$^+$-Oct6$^-$ ESCs expressing low or no Nanog, Otx2 should promote Nanog expression to re-direct these cells toward naive pluripotency or, alternatively, to keep them far from pre-primed-like identity switch (Figure 3G).

To further support these data, we also analyzed the expression of additional markers of the naive and primed states. Compared to WT, *Klf4*, *Esrrb*, *Fgf4*, and the phosphorylated active form of the LIF signaling transcriptional mediator Stat3 (p-Stat3) were all downregulated in Obs3 ESCs (Figures 3H and 3I), while the expression of epiblast markers, such as *Bmp2*, *T*, as well as p-Erk1,2 and p-Smad1,5,8, respectively the FGF- and BMP-signaling transducers, was upregulated (Figures 3H and 3I). *Fgf5*, a direct target of Otx2 in ESC transition toward EpiLCs (Buecker et al., 2014), was not induced in mutant ESCs in agreement with the fact that pre-primed-like cells were Otx2$^-$. We then tested the short-term response of Obs3 ESCs to LIF and Fgf. Compared to WT, mutant ESCs showed a higher and prolonged response to FGF and reduced activation of LIF signaling (Figures 3J and 3K). These findings support previous data indicating an expansion of the pre-primed-like and primed-like subtypes and a contraction of those with pre-naive-like and naive-like identity. Notably, these experiments (ALP staining, cell counting, and marker analysis) were consistently reproduced in an independently generated Obs3 mutant ESC line (data not shown).

Transcriptome Analysis of Obs3 Mutant ESCs

Previous studies have indicated that genes normally activated in primed cells are transcribed also in the ESC fraction susceptible to differentiation (Toyooka et al., 2008). We therefore predicted that, compared to WT, the transcriptome of Obs3 ESCs would be more similar to that of primed cells. A scatterplot representation of gene transcripts differentially expressed (up- and downregulated) in Obs3 ESCs (*Nanog*$^{\Delta Obs3/\Delta Obs3}$ ESCs versus WT ESCs) and d4 WT EpiSCs (WT EpiSCs versus WT ESCs) revealed that mutant ESCs showed an expression profile approaching their molecular identity to that of WT EpiSCs (Figure 4A; Table S6). Indeed, Obs3 mutant ESCs exhibited the expression of 626 upregulated and 395 downregulated genes in common with WT EpiSC-specific transcripts (Figures 4B and 4C; Table S6). A heatmap of these transcripts (626 and 395) showed that most of them are expressed at a level intermediate between WT EpiSCs and WT ESCs (Figure 4D), while the residual fraction appeared over-activated (8.8%) or over-repressed (10.4%) when compared to WT EpiSCs (Figure 4D). RT-PCR validation experiments performed for selected members of these gene categories showed that they tended to acquire the expression profile of WT EpiSCs (Figure 4E) and that this trend was even more pronounced for genes

(C–E) Otx2-binding profiles associated to *Nanog* (C), *Oct4* (D), and *Sox2* (E) loci in ESCs and EpiSCs, with highlighting (pink stripe) of the validated peaks, are shown.

(F–H) Schematic representation of the region upstream of the TSSs, showing for *Nanog* (F), *Oct4* (G), and *Sox2* (H) the extent of the peak and the Otx2 recognition sequences (Orss) identified within the peak. The horizontal arrows and associated letters identify the oligonucleotide pairs employed for ChIP validation assays; the Ors position upstream of the TSS is indicated by vertical numbers; the Orss within the peaks are sequentially numbered, in particular, 1 to 3 for *Nanog* and *Oct4* and 1 to 5 for *Sox2*.

(I and J) ChIP assays performed on ESCs (I) and d4 EpiSCs (J) for all the Orss identified within the peaks. Otx2 binding is reported as folds of enrichment compared to ESCs or EpiSCs null for *Otx2*.

See also Tables S1, S2, S3, and S4.

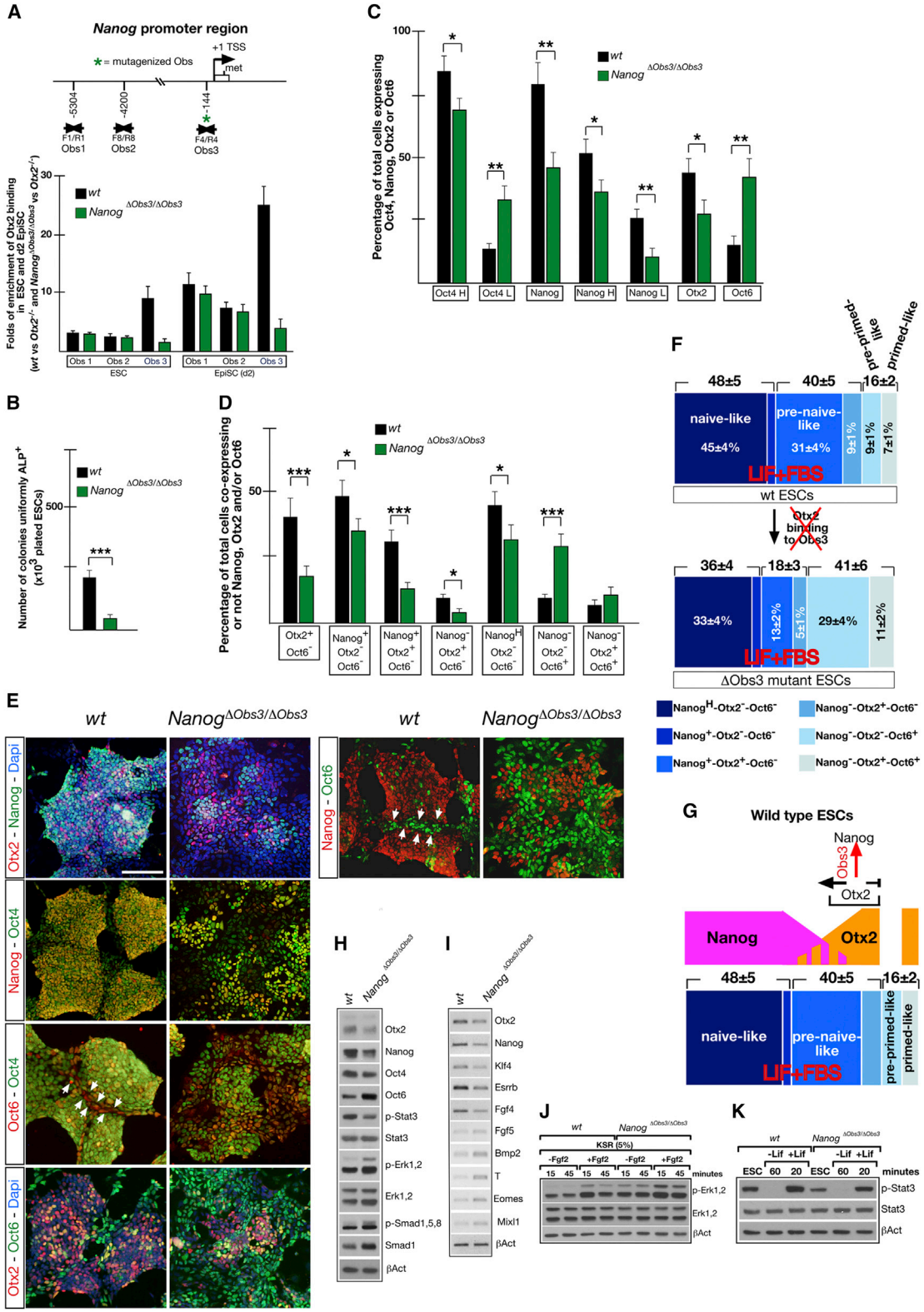

(legend on next page)

over-activated or over-repressed (Figure 4F). Thus, these findings show that a lack of Obs3 results in the activation of a primed-like molecular signature correlating with the expansion of the pre-primed-like and primed-like sub-compartments.

Chimerism of *Nanog*$^{\Delta Obs3/\Delta Obs3}$ ESCs Is Severely Impaired

Then we assayed whether the chimerism of Obs3 ESCs was impaired. Indeed, if mutant ESCs had significantly expanded the pre-primed-like subtype, their ability to colonize host blastocysts should be affected. Therefore, we generated *Nanog*$^{\Delta Obs3/\Delta Obs3}$; *R26*$^{GFP/+}$ ESCs, which enabled us to identify GFP$^+$ mutant ESCs in chimeric embryos. Compared to *R26*$^{GFP/+}$ control ESCs (Acampora et al., 2013), the ability of *Nanog*$^{\Delta Obs3/\Delta Obs3}$; *R26*$^{GFP/+}$ ESCs to generate chimeric embryos was severely affected (Figures 5A and 5B). Similarly, a lack of chimerism also was observed with *Nanog*$^{\Delta Obs3/\Delta Obs3}$ ESCs (Figure 5C).

Nanog$^{\Delta Obs3/\Delta Obs3}$ ESCs Exhibit an Improved Response to LIF Deprivation and Fgf2 Stimulation

Next we studied whether Obs3 ESCs can be primed more efficiently by LIF deprivation or Fgf2 addition compared to WT cells. Indeed, we found that, compared to WT, mutant ESCs exhibited a higher number of cells co-expressing Otx2 and Oct6 and a complementary marked reduction of Nanog$^+$ cells (Figure 5D). Moreover, compared to WT, in Obs3 ESCs, *Fgf5*, *T*, *Bmp2*, *Eomes*, *Foxa2*, and *Mixl1* were activated at a higher level (Figure 5E). These data indicate that the pre-primed-like cell population promptly responds to FGF-mediated activation of primed factors, including Otx2, to accomplish its transition into the primed state.

Nanog$^{\Delta Obs3/\Delta Obs3}$ ESCs Abnormally Respond to 2i/LIF-Mediated Conversion into the Naive State

Then we reverted the question and asked whether Obs3 ESCs may efficiently be converted into the naive state if cultured in N2B27 supplemented with LIF and 2i molecules. Obs3 ESCs were analyzed at passage 5 (P5), after transfer to the LIF/2i condition. Compared to WT, mutant ESCs generated fewer and much smaller Nanog$^+$-Oct4$^+$ pluripotent colonies and, unexpectedly, numerous Sox1$^+$-Tuj1$^+$ neuronal cells (Figure 5F). Further passages in LIF/2i medium, however, restored in mutant ESCs a phenotype very similar to that of WT ESCs, likely due to the selective expansion of the initially small fraction of naive cells. In addition, both WT and mutant ESCs lacked Otx2 and Oct6 expression in 2i/LIF (Figure 5F). However, when returned to FBS/LIF, WT and mutant ESCs restored expression of Otx2 and Oct6 (Figure 5F). Thus, Obs3 ESCs resist for several passages to efficient conversion into naive pluripotency, and transiently a large fraction of them, possibly those with pre-primed-like identity, differentiates into neural cells. Thus, these and previous findings suggest that Obs3 mutant ESCs are a mixture of naive ESCs and EpiSCs.

Obs3 EpiSCs Exhibit Abnormalities in Proliferation, Identity, and Mesendoderm Differentiation

Since Otx2 showed robust binding to Obs3 in EpiSCs, we studied whether also the generation and identity of Obs3 EpiSC colonies were affected. Compared to WT, d4 mutant EpiSC colonies were remarkably larger in size and exhibited sharp borders and compact morphology (Figure 6A). Analysis of apoptotic cell death and mitotic index showed a substantial decrease of active Caspase3$^+$ (act-Casp3) cells and a 2-fold increase of phospho-Histone3$^+$ (p-H3) cells (Figures 6A and 6B; Table S7), suggesting that reduced apoptosis and contemporary hyperproliferation may be responsible for increased size of mutant EpiSC colonies. Furthermore, compared to WT, in mutant EpiSCs, Nanog was downregulated, Otx2 and Oct6 were upregulated, Oct4 and *Fgf5* were unaffected, and the expression of mesendoderm markers (e.g., T, Foxa2, *Chordin* [*Chd*], *Mixl1*, *Gata4*, and *Gata6*) was diminished (Figures 6C–6E). In particular,

Figure 3. Obs3 Is Required to Maintain Integrity of the ESC State

(A) ChIP assays show that Otx2 binding to Obs3 is abolished in Obs3 mutant ESCs and EpiSCs, while the binding to Obs1 and Obs2 is unaffected.

(B) Graphic representation shows that the number of Obs3 ESC colonies uniformly expressing ALP is diminished (***$p < 0.001$).

(C and D) Cell-counting data show the percentage of total cells expressing Oct4, Nanog, Otx2, and Oct6 (C) or expressing different combinations of Otx2, Nanog, and Oct6 (D) (*$p = 0.001$, **$p < 0.001$, and ***$p < 0.001$).

(E) Immunohistochemistry experiments showing in WT and *Nanog*$^{\Delta Obs3/\Delta Obs3}$ ESCs the expression of Otx2 and Nanog, Nanog and Oct4, Oct6 and Oct4, Nanog and Oct6, and Otx2 and Oct6. In some immunohistochemistry experiments cells also are stained with DAPI. Scale bar, 100 μm.

(F and G) The ESC state is characterized by cell heterogeneity and the co-existence of different cell subtypes (F). Through our marker analysis, we identified, in WT ESCs cultured in LIF/FBS, three major Oct4$^+$ ESC compartments: the first is Nanog$^+$-Otx2$^-$-Oct6$^-$, accounts for 48% of total ESCs, and is prevalently composed by Nanog^H-Otx2$^-$-Oct6$^-$ naive-like cells (45 ± 4) (dark blue); the second is Oct6$^+$, accounts for 16% of total cells, and includes two small sub-compartments, the Nanog$^-$-Otx2$^-$-Oct6$^+$ pre-primed-like (9 ± 1) (pale blue) and the Nanog$^-$-Otx2$^+$-Oct6$^+$ primed-like (7 ± 1) (light pale blue); and the third is Otx2$^+$-Oct6$^-$, accounts for 40% of total cells, and includes a large Nanog$^+$-Otx2$^+$-Oct6$^-$ pre-naive-like (31 ± 4) sub-compartment (blue) and a small Nanog$^-$-Otx2$^+$-Oct6$^-$ (9 ± 1) sub-compartment (light blue). Loss of Obs3 generates a remarkable size re-organization primarily affecting the pre-primed-like and pre-naive-like sub-compartments, which, compared to WT, are respectively expanded and contracted. (G) Our data suggest that, in the Otx2$^+$-Oct6$^-$ compartment and in particular in ESCs expressing high Otx2 and low or no Nanog, Obs3 is required for Otx2 to re-activate/enhance Nanog expression. This event should prevent identity switch of pre-naive-like and Nanog$^-$-Otx2$^+$-Oct6$^-$ ESC subtypes into pre-primed-like subtype and promote progression toward the naive-like identity. The color codes are indicated in (F); the presumptive expression level for Nanog and Otx2 is shown in magenta and orange, respectively (G).

(H and I) Western blot (H) and RT-PCR assays (I) show that, compared to WT, Obs3 ESCs exhibit reduced levels of Otx2, Nanog, Oct4, *Klf4*, *Esrrb*, and *Fgf4* and increased expression of Oct6; a moderate increase is observed also for epiblast markers, such as *T*, *Bmp2*, *Eomes*, and *Mixl1*, while *Fgf5* expression is unaffected (I). The assessment of LIF-, FGF-, and BMP-signaling pathways shows that Obs3 ESCs exhibit increased levels of p-Erk1,2 and p-Smad1,5,8 and a reduction of p-Stat3 (H).

(J and K) Compared to WT, Obs3 mutant ESCs show a higher and prolonged response to Fgf2 addition after brief starvation in 5% KSR (J) and, instead, a less efficient response to LIF (K).

See also Figures S1 and S2 and Table S5.

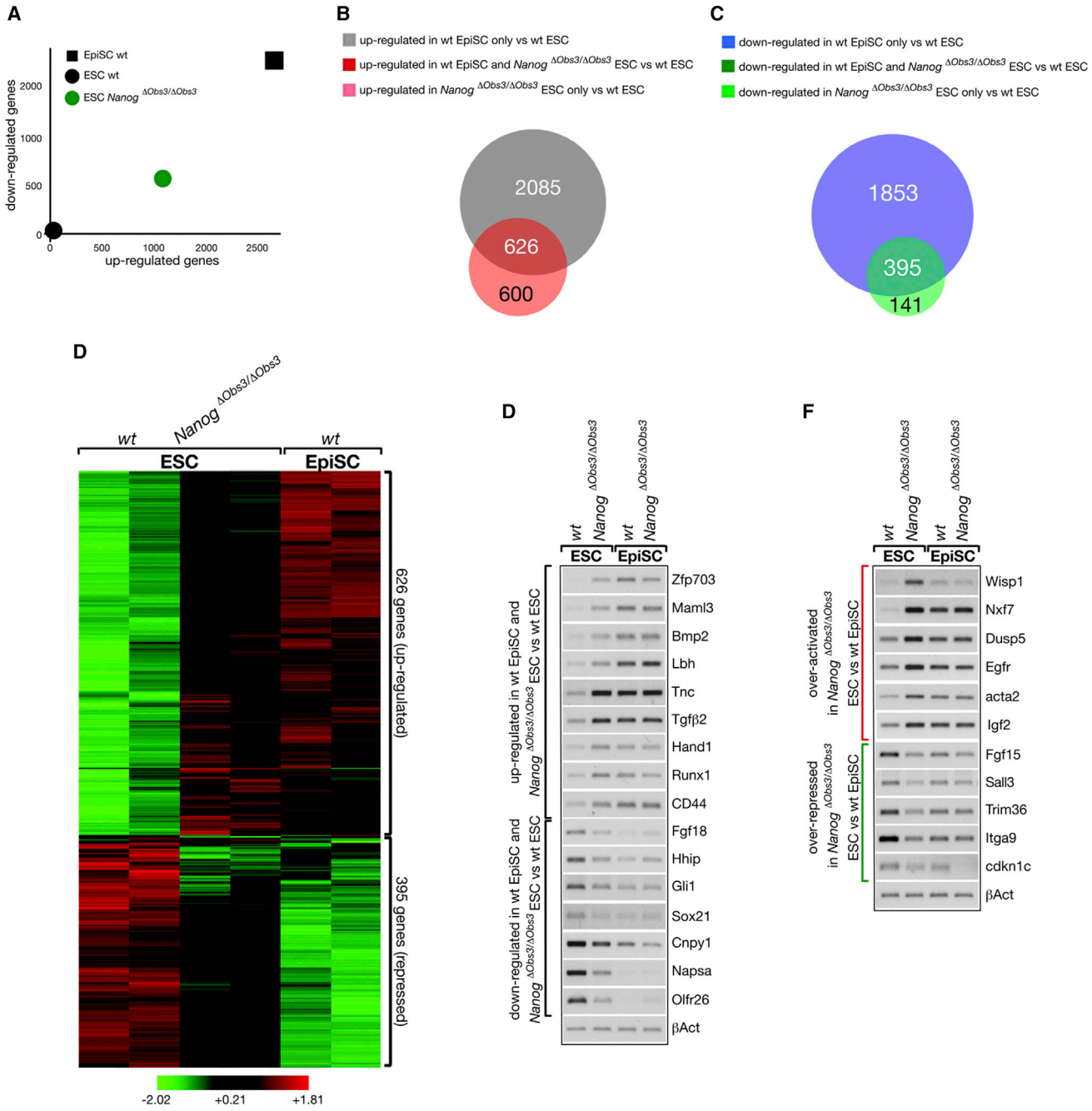

Figure 4. The Transcriptome of Obs3 Mutant ESCs Exhibits a Molecular Signature Approaching that of Primed EpiSCs

(A) Scatterplot shows the number of upregulated (x axis) and downregulated (y axis) genes, as deduced by comparing WT EpiSCs (black square) versus WT ESCs (black dot) and *Nanog*$^{\Delta Obs3/\Delta Obs3}$ ESCs (green dot) versus WT ESCs.

(B and C) Venn diagrams show the number of genes upregulated (B) and downregulated (C) in Obs3 ESCs and WT EpiSCs.

(D) Heatmap shows the upregulated (626) and downregulated (395) genes shared by WT EpiSCs and *Nanog*$^{\Delta Obs3/\Delta Obs3}$ ESCs.

(E and F) Validation assays were performed on WT and Obs3 ESCs and d4 EpiSCs for selected genes upregulated or downregulated at intermediate level (E) or for those over-activated or over-repressed (F).

See also Table S6.

immunohistochemistry assays showed that T and Foxa2 were expressed in restricted subregions of EpiSC colonies (Figure 6C) or often not expressed at all. Analysis of FGF, BMP, and WNT pathways showed that the levels of p-Erk1,2; p-Smad1,5,8; phospho-β-catenin; and active-β-catenin were unaffected (Figure 6D). Therefore, these data suggest that Obs3-dependent

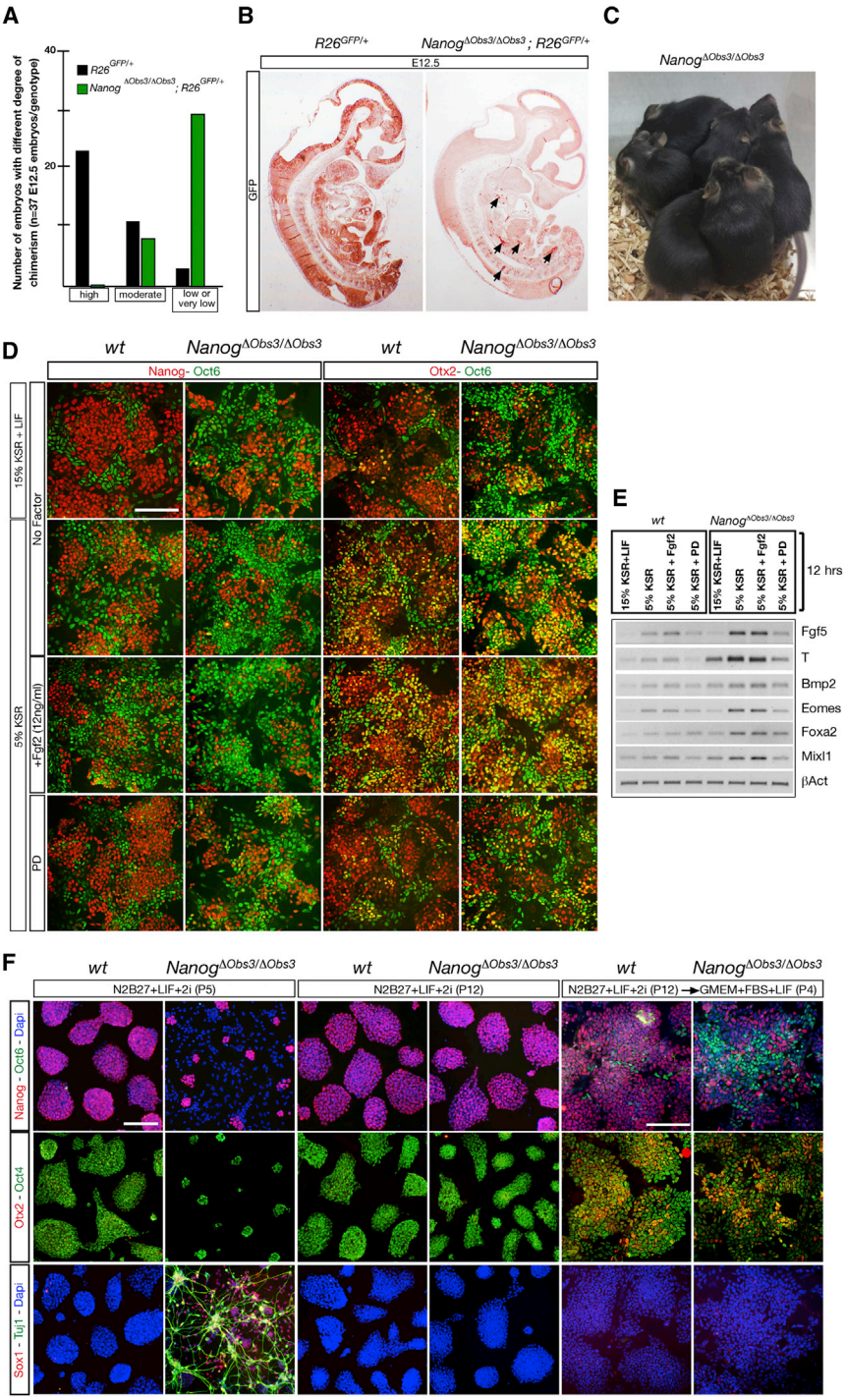

Figure 5. *Nanog*$^{\Delta Obs3/\Delta Obs3}$ ESCs Exhibit Impaired Chimerism and Enhanced Response to Fgf2

(A–C) Embryos injected with *Nanog*$^{\Delta Obs3/\Delta Obs3}$; *R26*$^{GFP/+}$ mutant and *R26*$^{GFP/+}$ control ESCs are analyzed at E12.5 for detection of GFP$^+$ cells (A); the arrows in (B) point to sporadic small groups of GFP$^+$ cells; impaired chimerism is evident also with *Nanog*$^{\Delta Obs3/\Delta Obs3}$ ESCs (C).

(D and E) Immunohistochemistry (D) and RT-PCR assays (E) were performed on WT and *Nanog*$^{\Delta Obs3/\Delta Obs3}$ ESCs, cultured for 12 hr in 15% KSR + LIF, in 5% KSR without LIF, or in 5% KSR supplemented with Fgf2 or PD, to assess the distribution of Nanog, Otx2, and Oct6 (D) and the expression of *Fgf5*, *T*, *Bmp2*, *Eomes*, *Foxa2*, and *Mixl1* (E).

(F) Immunohistochemistry assays performed on WT and Obs3 ESCs cultured in LIF/2i show that Obs3 ESCs exhibit (at P5) small ESC colonies expressing Nanog and Oct4 and many Sox1$^+$-Tuj1$^+$ neural cells; however, at P12, WT and Obs3 ESCs are very similar. When re-plated in LIF/FBS, WT and Obs3 ESCs revert to their original identities. Scale bars, 100 μm.

functions also are required in EpiSCs to control their identity, proliferation, and differentiation.

Otx2 Binding to Obs3 Is Required for the Differentiation of ICM-Derived Epiblast Lineage

Next we investigated whether the Otx2 binding to Obs3 is required also in vivo to support the naive pluripotency network controlling epiblast specification. *Nanog*$^{\Delta Obs3/\Delta Obs3}$ mutant mice were healthy and fertile, but, compared to WT, the number of mice per litter was reduced by about 50% (Figure S3A). This reduction also was observed at E12.5 and E6.5; at E4 the number of embryos per litter was yet diminished by about 25%, and only at E2.5 was it close to that of WT (Figure S3A). This suggested two temporal windows of preimplantation lethality: the first before E4 and the second between E4 and implantation. Immunohistochemistry experiments between E5.5 and E6.7, with markers for extraembryonic ectoderm (Oct6), epiblast (Otx2, Oct4, Nanog, and Oct6), extraembryonic endoderm derivatives (Gata4, Foxa2, and Otx2), and primitive streak (T and Foxa2), showed no evident abnormalities in Obs3 mutants (Figure S3B). Conversely, at early/mid-morula stage, Obs3 mutants exhibited a heterogeneous phenotype: 24% of mutants were similar to WT embryos; 13% showed degenerating blastomeres with the loss of Nanog, Otx2, and Gata6 expression; and 62% exhibited either a severe loss (28%) or a less drastic but evident reduction (34%) of cells expressing a high level of Nanog (Figures 7A and S4A; Table S8). Apparently, the expression of Otx2 and Gata6 was unaffected (Figures 7A and S4A).

In early blastocysts Nanog was downregulated in many ICM cells (Figure 7B). At E3.75–E4, 71% of mutant blastocysts

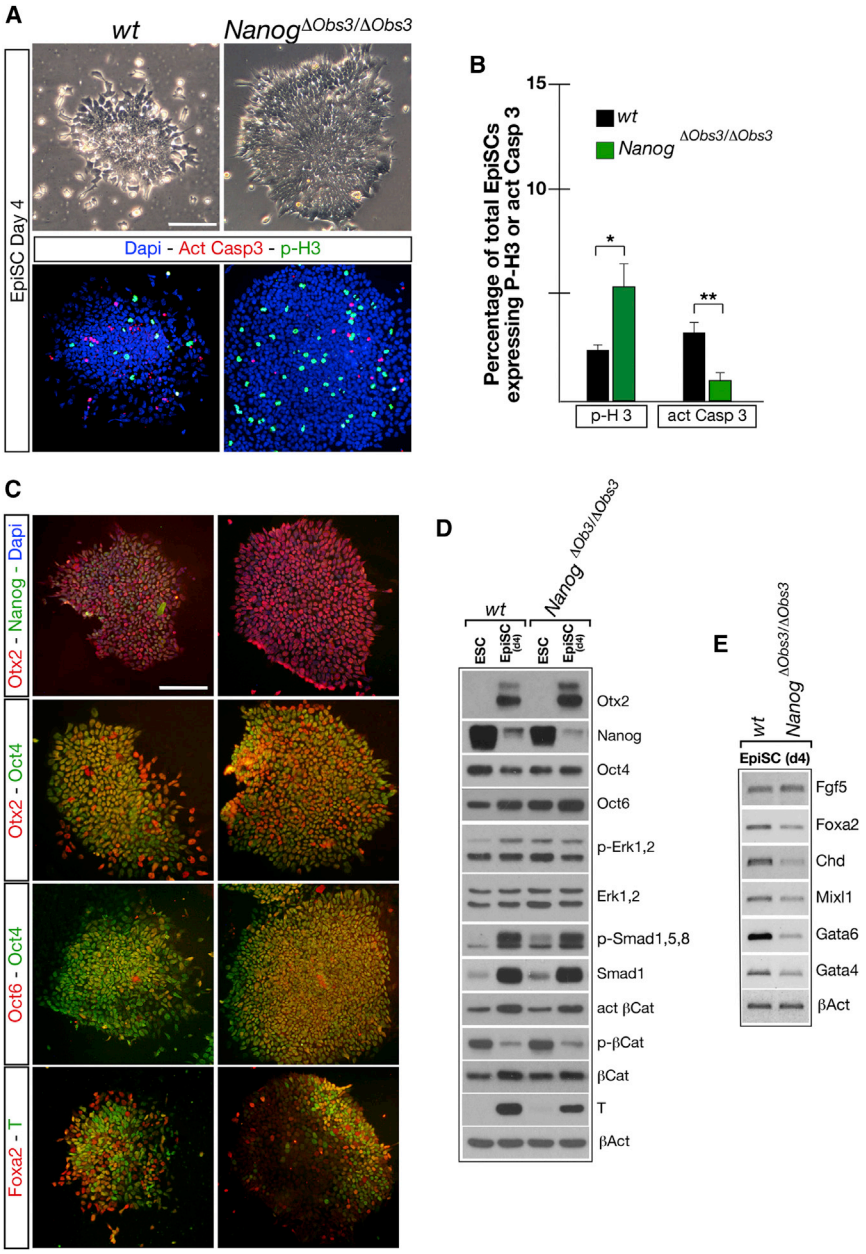

Figure 6. *Nanog*$^{\Delta Obs3/\Delta Obs3}$ EpiSCs Exhibit Abnormalities in Proliferation, Apoptosis, and Mesendoderm Differentiation

(A and B) Morphology inspection, immunohistochemistry assays with act-Casp3 and p-H3 (A), and cell counting of p-H3$^+$ and act-Casp3$^+$ cells (B) are shown (*p = 0.001 and **p < 0.001).

(C–E) Immunohistochemistry (C), western blot (D), and RT-PCR (E) experiments reveal that, compared to WT, in Obs3 EpiSCs Nanog is downregulated; Otx2 and Oct6 are upregulated (C and D); T, *Foxa2*, *Chd*, *Mixl1*, *Gata6*, and *Gata4* mesendoderm markers are diminished (C–E); and Oct4, *Fgf5*, p-Erk1,2, act-β-cat, p-β-cat, and p-Smad1,5,8 are unmodified (D). Scale bars, 100 μm.

See also Table S7.

exhibited abnormal expression of Nanog and Gata4 (Figures 7C and S4B; Table S8). Indeed, while the expression of Oct4, Cdx2, and Otx2 was unaffected, Nanog was detected in few epiblast cells and Gata4 expanded to Nanog$^-$ presumptive epiblast cells. At E4.7–E4.9, a total of 42% of Obs3 mutants showed severe abnormalities in molecular identity and/or morphology. Indeed, Gata4 was detected in many cells distributed in the epiblast region, while Otx2 and Oct6 were expressed in a remarkably diminished number of epiblast cells complementary to those Gata4$^+$ (Figures 7D and S4C). These Otx2$^+$-Oct6$^+$ cells should correspond to the progeny of the few Nanog$^+$ epiblast cells detected at E3.75–E4. As for the rest of mutant embryos, 31% of them exhibited a moderate reduction in the number of Otx2$^+$ cells and a corresponding increase of Gata4$^+$ cells, and 25% of them displayed a fairly normal morphology (Figure S4C). Based on these findings, we hypothesized that Otx2-null mutants should exhibit abnormalities in common with *Nanog*$^{\Delta Obs3/\Delta Obs3}$ embryos. In this context, although *Otx2*$^{-/-}$ embryos exhibit moderate de-repression of Nanog in postimplantation epiblast (Acampora et al., 2013), little is known about their preimplantation phenotype. We found that, at E3.75–E4 and E4.7–E4.9, about 50% of *Otx2*$^{-/-}$ embryos showed abnormalities very similar to those detected in Obs3 mutants (Figure S5). At E3.75–E4, *Otx2*$^{-/-}$ mutants with normal expression of Gata4 exhibited an apparently unaffected expression of Nanog (data not shown); instead at E4.7–E4.9, compared to WT, five of nine mutants showed upregulation of Nanog in most epiblast cells (Figure S5B). This abnormality was never observed in Obs3 mutants.

Collectively, our data indicate that Otx2 contributes (1) at mid- to late morula stage to program subsequent differentiation of the ICM into epiblast through Obs3-mediated control of Nanog expression, and (2) between E4 and E4.7 to efficiently downregulate Nanog. However, the phenotype variability of Obs3 mutants suggests the existence of compensatory mechanism(s) ensuring embryo survival.

DISCUSSION

We have investigated the role of the Otx2 transcriptional network in the control of the ESC state. We identified Oct4, Sox2, and Nanog as direct targets of Otx2, and we studied the functional relevance of the Otx2 binding to the proximal promoter region of Nanog. Loss of Obs3 generates a new ESC

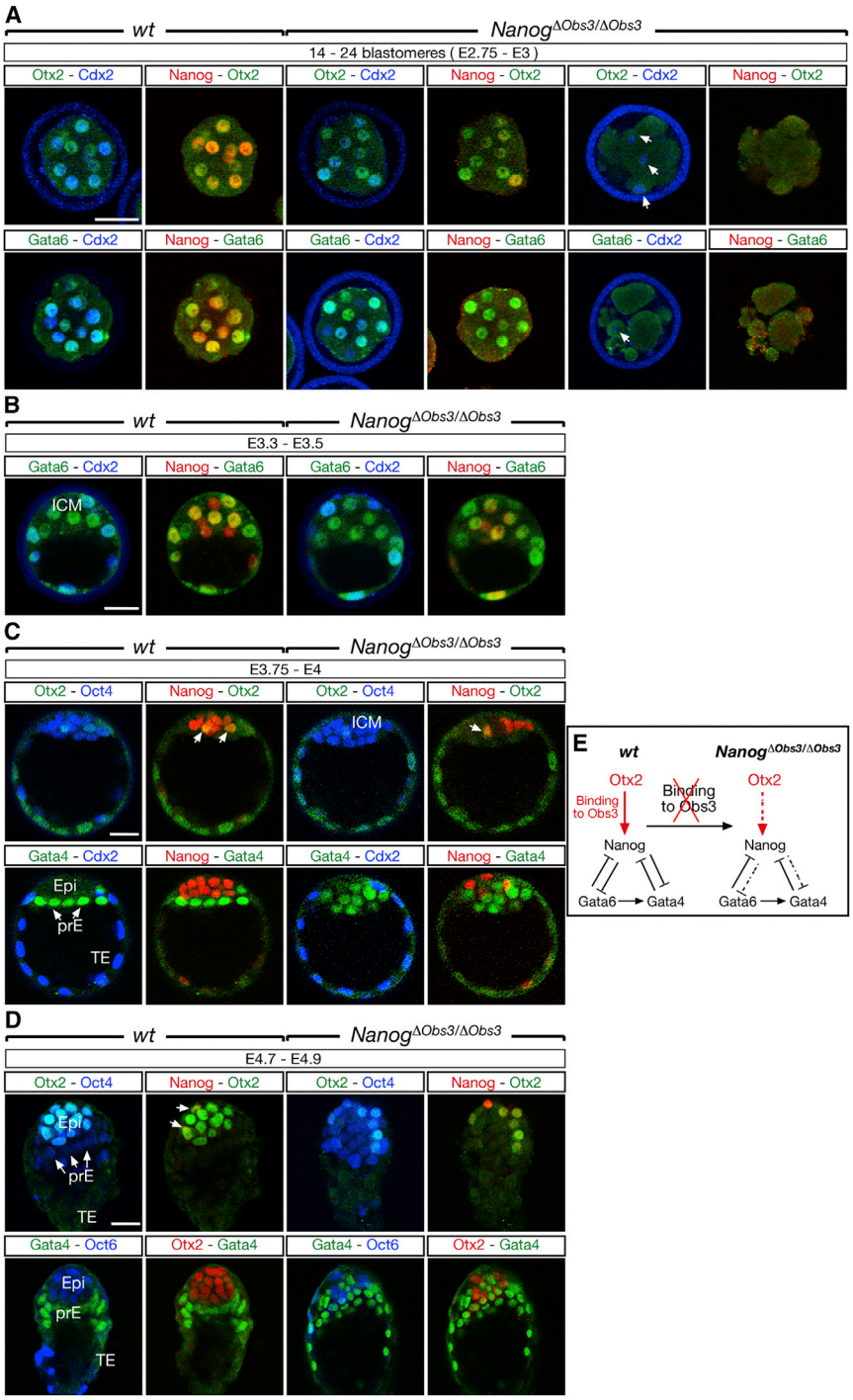

Figure 7. Obs3 Mutant Embryos Exhibit Severe Impairment in Differentiation of ICM-Derived Epiblast Lineage

(A) Immunostaining with Otx2, Nanog, and Cdx2 and with Gata6, Nanog, and Cdx2 shows that, at mid-morula (14–24 blastomeres), most of *Nanog*$^{\Delta Obs3/\Delta Obs3}$ mutants strongly attenuate Nanog expression, while the expression of Gata6, Otx2, and Cdx2 appears unchanged. A fraction of Obs3 mutants exhibits a very strong phenotype with loss of all markers except occasional staining with Cdx2 (arrows).

(B) Immunostaining with Gata6, Nanog, and Cdx2 shows that, at E3.3–E3.5, mutant embryos confirm the reduced expression of Nanog.

(C) Immunostaining with Otx2, Nanog, and Oct4 and with Gata4, Nanog, and Cdx2 shows that, at E3.75–E4 in most of Obs3 mutants, Nanog is detected in a reduced number of Oct4^{+} epiblast cells and Gata4 is expanded to most of Nanog^{-} presumptive epiblast cells.

(D) Immunostaining with Otx2, Nanog, and Oct4 and with Gata4, Otx2, and Oct6 shows that, at E4.7–E4.9, the majority of *Nanog*$^{\Delta Obs3/\Delta Obs3}$ embryos, although abnormal in morphology and Gata4 expression, activate Otx2 and Oct6 in the residual Gata4^{-}-Oct4^{+} epiblast cells. Nanog is sporadically expressed only in some Otx2^{+} cells.

(E) Schematic representation integrating our data (in red) with those previously reported (in black) shows that, during ICM differentiation of prE and epiblast, loss of Obs3 affects Nanog expression in ICM precursors of epiblast (dashed arrow); a reduced level of Nanog results in decreased efficiency to repress Gata4/6 factors (dashed suppression symbol) and consequent epiblast into prE identity switch. Abbreviations are as in previous Figures. Scale bars, 30 μm.

See also Figures S3–S5 and Table S8.

steady state characterized by a size re-distribution of ESC-subtype compartments; overall this new steady state exhibits increased similarities to primed pluripotent cells, although a naive component is retained. We also show that in vivo loss of Obs3 causes downregulation of Nanog expression at morula stage and abnormal differentiation of the ICM-derived epiblast lineage.

Otx2 Controls the Identity and Number of Specific ESC Subtypes by Binding to the Nanog Promoter

The mechanism that controls pluripotency in naive and primed stem cells has allowed the identification of regulatory networks that instruct pluripotent stem cells on how to establish and maintain their state and how to direct cell lineage decisions or transition between different pluripotent states (Kalmar et al., 2009; Hanna et al., 2010; Lanner and Rossant, 2010; Spitz and Furlong, 2012; Kalkan and Smith, 2014; Torres-Padilla and Chambers, 2014). In this study we have investigated the role of the Otx2 binding to the Nanog promoter, a specific branch of the Otx2 transcriptional network. We have shown that, in LIF/FBS growth conditions, loss of this specific branch affects the integrity of ESC-subtype compartments. Indeed, Obs3 mutant ESCs exhibit severe abnormalities mainly affecting the size of two specific ESC subtypes, which we called the

pre-naive-like (Nanog^{+}-Otx2^{+}-Oct6^{-}-Oct4^{+}) and the pre-primed-like (Nanog^{-}-Otx2^{-}-Oct6^{+}-Oct4^{+}) ESCs. Compared to WT, the number of pre-naive-like ESCs was diminished while that of pre-primed-like cells remarkably expanded. To a lesser extent, also the naive-like and the primed-like subtypes were respectively reduced and expanded (Figure 3F).

We suggest that abnormalities detected in Obs3 mutant ESCs should originate prevalently in the pre-naive-like sub-compartment, which exhibits graded distribution of complementary levels of Otx2 and Nanog, and in the Nanog^{-}-Otx2^{+}-Oct6^{-} unassigned sub-compartment (Figure 3G). We propose that Otx2 contributes to activating/sustaining Nanog expression, in cells co-expressing high Otx2 and low or no Nanog, to allow re-directioning of cell identity toward the naive subtype (Figure 3G). It remains to be clarified whether a high level of Nanog may subsequently repress Otx2 to allow full progression into the naive-like subtype; in this context, our data indicate that in ESCs Nanog may efficiently bind the Otx2 promoter region (data not shown). In summary, our data uncover a mechanism that contributes to maintaining the integrity of the ESC steady state by preventing an identity switch of the pre-naive-like into the pre-primed-like subtype. This mechanism also may contribute to the metastable condition of ESCs grown in LIF/FBS by regulating cell heterogeneity among transitional sub-compartments of pluripotency, and it is dispensable in LIF/2i culture conditions where naive pluripotency becomes unimodal and Otx2 expression suppressed (Hayashi et al., 2008; Kalmar et al., 2009; Silva et al., 2009; Faddah et al., 2013; Torres-Padilla and Chambers, 2014; Ohnishi et al., 2014). Interestingly, Obs3 mutant ESCs do not exhibit an irreversible and progressive conversion into the pre-primed-like subtype, rather they establish a new steady-state equilibrium characterized by a new size representation of internal subtype compartments (Figure 3F), which may imply the existence of progressive states of pluripotency.

Otx2, Nanog, and Oct6 Expression in Preimplantation Embryos Identifies Three Stage-Specific Expression Profiles of the Epiblast

In preimplantation embryos at mid- to late morula and early blastocyst stages, Otx2 is detected at a high level prevalently in Nanog^{+} cells of the ICM; from E3.5, Otx2 expression is gradually downregulated in the epiblast where, from E3.7 to E4.5, it is virtually absent. Conversely, from E4.5 onward, Nanog is downregulated and Otx2 together with Oct6 rapidly activated in the epiblast, which exhibits overt similarity with that of early postimplantation embryos. This suggests that transition of naive into primed pluripotency may occur before implantation. Furthermore, together with previous studies (Silva and Smith, 2008; Silva et al., 2009; Najm et al., 2011; Acampora et al., 2013; Martinez Arias et al., 2013; Torres-Padilla and Chambers, 2014; Boroviak et al., 2014), our data suggest three stage-specific expression profiles of the epiblast: the first, between E3.5 and E4.5, is dominated by a high level of Nanog and a low level of Otx2 and exhibits ground-state naive pluripotency and marked similarity to ESCs cultured in LIF/2i; the second, between E4.5 and E4.7, is characterized by contemporary and frequently complementary expression of Nanog and Otx2 and resembles the identity of ESCs cultured in LIF/FBS; and the third, between E4.7 and implantation, is characterized by a low level or no expression of Nanog and high levels of Otx2 and Oct6, may correspond to the initial primed state, and is markedly similar to that of early EpiLCs.

Obs3-Dependent Control of Nanog Expression by Otx2 Modulates ICM Differentiation of the Epiblast

Previous studies indicated that mutual antagonism between Nanog and Gata6 is an essential aspect of ICM differentiation into epiblast and prE (Kwon et al., 2008; Frankenberg et al., 2011; Grabarek et al., 2012; Martinez Arias et al., 2013; Ohnishi et al., 2014; Hermitte and Chazaud, 2014; Bessonnard et al., 2014; Schrode et al., 2014). In these studies, the loss of Nanog results in an expansion of the Gata6^{+} prE lineage at the expense of the epiblast. However, in these studies, the factor(s) required to activate/maintain Nanog expression before and during ICM differentiation remained elusive. Our data show that, in the majority (>70%) of mutant embryos, Otx2 is required through Obs3 to activate/sustain Nanog expression at mid- to late morula stage to predispose ICM for differentiation of the epiblast cell lineage. Coherently, about 50% of Otx2-null mutants exhibit similar abnormalities. Therefore, the loss of Obs3 or Otx2 results in early downregulation of Nanog and inefficient antagonism of Gata6/4 expression with consequent identity switch of ICM-derived epiblast precursors into prE (Figure 7E). Thus, the Obs3-dependent control of Nanog expression by Otx2 may trigger early cell lineage specification in mammalian development. Furthermore, since the analysis of *Otx2*$^{-/-}$ embryos indicates that after E4 Otx2 is required also to downregulate Nanog in the epiblast, together these data suggest that, during blastocyst development, Otx2 and Nanog impart complementary and inter-dependent instructions controlling initial specification of naive epiblast and, subsequently, its transition to primed pluripotency. However, the finding that Obs3 mutants do not exhibit a fully penetrant phenotype suggests the existence of a possible backup system partially compensating for the loss of Obs3.

EXPERIMENTAL PROCEDURES

Generation of Obs3 Mutant ESCs and Mouse Strain

The Obs3 mutation was introduced in the *Nanog*$^{\Delta Obs3}$-targeting vector by PCR-mediated mutagenesis (Figure S1A). Targeting of the construct was done into the E14Tg2a ESC line (Figures S1B and S1C). One *Nanog*$^{\Delta Obs3/+}$ ESC clone was either injected into C57BL6 blastocysts to establish a mutant mouse colony or re-targeted to obtain a *Nanog*$^{\Delta Obs3/\Delta Obs3}$ ESC line. Genotyping was performed with allele-specific primers (Figure S1D; Table S9). Targeting of the GFP gene in the *Rosa26* locus of *Nanog*$^{\Delta Obs3/\Delta Obs3}$ ESCs was performed as reported (Acampora et al., 2013). Animals were handled in accordance with the authorization 1196/2015-PR released by the Italian Ministry of Health.

Cell Culture Experiments and ALP Assays

E14Tg2a WT and Obs3 mutant ESCs were grown in Glasgow minimal essential medium (GMEM) plus fetal bovine serum (FBS) (HyClone) and LIF (Millipore). As for the experiments involving 2i, ESCs grown in FBS/LIF were plated in N2B27 medium supplemented with LIF, MEK1/2 inhibitor PD325901 (PD), and GSK3 inhibitor CHIR99021 (CHIR) (both from Calbiochem) (LIF/2i medium) (Buecker et al., 2014). These cells were referred to as P1 and were propagated every 3 days by accutase treatment up to P12. EpiSCs were induced from ESCs as previously described (Brons et al., 2007; Acampora et al., 2013) and analyzed at d4. Response of WT and *Nanog*$^{\Delta Obs3/\Delta Obs3}$ ESCs to LIF and

Fgf2 starvation/re-stimulation was assayed as previously described (Zhang et al., 2010; Acampora et al., 2013). ALP assays were performed as previously described (Acampora et al., 2013). The number of ESC colonies and SD were calculated in four independent assays, and p value was determined by using the one-tailed Student's t test.

RT-PCR and Western Blotting

RT-PCRs were performed in non-saturating conditions using primers and cycles listed in Table S9. Western blots were probed with antibodies as previously described (Acampora et al., 2013), with the addition of rabbit antibodies against p-β-catenin (1:750) and βcat (1:1,000) (Cell Signaling Technology) and mouse antibodies against Oct6 (1:600) and act-β-catenin (1:750) (Millipore).

Cell Counting, Chimerism Experiments, and Immunohistochemistry

Detailed descriptions are provided in the Supplemental Experimental Procedures.

ChIP-Seq Experiments, ChIP Assays, and ChIP-Seq Data Analysis

Detailed descriptions are provided in the Supplemental Experimental Procedures.

RNA-Seq Experiments, Analysis of RNA-Seq Data, Heatmap Representation, and RNA-Seq Validation Assays

Detailed descriptions are provided in the Supplemental Experimental Procedures.

ACCESSION NUMBERS

The accession number for the RNA sequencing (RNA-seq) and ChIP-seq data reported in this paper is ArrayExpress: E-MTAB-3856.

SUPPLEMENTAL INFORMATION

Supplemental Information includes Supplemental Experimental Procedures, five figures, and nine tables and can be found with this article online at http://dx.doi.org/10.1016/j.celrep.2016.05.041.

AUTHOR CONTRIBUTIONS

D.A. performed and analyzed most of the in vitro and in vivo experiments. D.O. performed experiments on EpiSCs and analyzed chimeric embryos. G.P. analyzed ChIP-seq data. A.G., M.S., and V.N. performed and analyzed RNA-seq experiments. L.G.D.G. performed validation experiments for RNA-seq and ChIP assays and managed mouse colonies. A.S. conceived the experiments, interpreted the data with D.A., and wrote the manuscript.

ACKNOWLEDGMENTS

We thank M. Autiero, E. Boncinelli, I. Chambers, and C. Stern for critical reading of the manuscript and helpful discussion; D. Graniero for typing and formatting the manuscript; and the staffs of IGB animal house facility, the CEINGE confocal microscopy facility, and the Tigem NGS facility. This work was supported by the Italian Association for Cancer Research (AIRC) (Project IG-14152) and POR MOVIE of Regione Campania.

Received: January 30, 2016
Revised: March 12, 2016
Accepted: May 9, 2016
Published: June 9, 2016

REFERENCES

Acampora, D., Di Giovannantonio, L.G., and Simeone, A. (2013). Otx2 is an intrinsic determinant of the embryonic stem cell state and is required for transition to a stable epiblast stem cell condition. Development *140*, 43–55.

Bessonnard, S., De Mot, L., Gonze, D., Barriol, M., Dennis, C., Goldbeter, A., Dupont, G., and Chazaud, C. (2014). Gata6, Nanog and Erk signaling control cell fate in the inner cell mass through a tristable regulatory network. Development *141*, 3637–3648.

Boroviak, T., Loos, R., Bertone, P., Smith, A., and Nichols, J. (2014). The ability of inner-cell-mass cells to self-renew as embryonic stem cells is acquired following epiblast specification. Nat. Cell Biol. *16*, 516–528.

Brons, I.G., Smithers, L.E., Trotter, M.W., Rugg-Gunn, P., Sun, B., Chuva de Sousa Lopes, S.M., Howlett, S.K., Clarkson, A., Ahrlund-Richter, L., Pedersen, R.A., and Vallier, L. (2007). Derivation of pluripotent epiblast stem cells from mammalian embryos. Nature *448*, 191–195.

Buecker, C., Srinivasan, R., Wu, Z., Calo, E., Acampora, D., Faial, T., Simeone, A., Tan, M., Swigut, T., and Wysocka, J. (2014). Reorganization of enhancer patterns in transition from naive to primed pluripotency. Cell Stem Cell *14*, 838–853.

Chambers, I., Silva, J., Colby, D., Nichols, J., Nijmeijer, B., Robertson, M., Vrana, J., Jones, K., Grotewold, L., and Smith, A. (2007). Nanog safeguards pluripotency and mediates germline development. Nature *450*, 1230–1234.

Evans, M.J., and Kaufman, M.H. (1981). Establishment in culture of pluripotential cells from mouse embryos. Nature *292*, 154–156.

Faddah, D.A., Wang, H., Cheng, A.W., Katz, Y., Buganim, Y., and Jaenisch, R. (2013). Single-cell analysis reveals that expression of nanog is biallelic and equally variable as that of other pluripotency factors in mouse ESCs. Cell Stem Cell *13*, 23–29.

Festuccia, N., Osorno, R., Halbritter, F., Karwacki-Neisius, V., Navarro, P., Colby, D., Wong, F., Yates, A., Tomlinson, S.R., and Chambers, I. (2012). Esrrb is a direct Nanog target gene that can substitute for Nanog function in pluripotent cells. Cell Stem Cell *11*, 477–490.

Frankenberg, S., Gerbe, F., Bessonnard, S., Belville, C., Pouchin, P., Bardot, O., and Chazaud, C. (2011). Primitive endoderm differentiates via a three-step mechanism involving Nanog and RTK signaling. Dev. Cell *21*, 1005–1013.

Grabarek, J.B., Zyzyńska, K., Saiz, N., Piliszek, A., Frankenberg, S., Nichols, J., Hadjantonakis, A.K., and Plusa, B. (2012). Differential plasticity of epiblast and primitive endoderm precursors within the ICM of the early mouse embryo. Development *139*, 129–139.

Greber, B., Wu, G., Bernemann, C., Joo, J.Y., Han, D.W., Ko, K., Tapia, N., Sabour, D., Sterneckert, J., Tesar, P., and Schöler, H.R. (2010). Conserved and divergent roles of FGF signaling in mouse epiblast stem cells and human embryonic stem cells. Cell Stem Cell *6*, 215–226.

Hanna, J.H., Saha, K., and Jaenisch, R. (2010). Pluripotency and cellular reprogramming: facts, hypotheses, unresolved issues. Cell *143*, 508–525.

Hayashi, K., Lopes, S.M., Tang, F., and Surani, M.A. (2008). Dynamic equilibrium and heterogeneity of mouse pluripotent stem cells with distinct functional and epigenetic states. Cell Stem Cell *3*, 391–401.

Hermitte, S., and Chazaud, C. (2014). Primitive endoderm differentiation: from specification to epithelium formation. Philos. Trans. R. Soc. Lond. B Biol. Sci. *369*, 20130537.

Kalkan, T., and Smith, A. (2014). Mapping the route from naive pluripotency to lineage specification. Philos. Trans. R. Soc. Lond. B Biol. Sci. *369*, 20130540.

Kalmar, T., Lim, C., Hayward, P., Muñoz-Descalzo, S., Nichols, J., Garcia-Ojalvo, J., and Martinez Arias, A. (2009). Regulated fluctuations in nanog expression mediate cell fate decisions in embryonic stem cells. PLoS Biol. *7*, e1000149.

Kunath, T. (2011). Primed for pluripotency. Cell Stem Cell *8*, 241–242.

Kwon, G.S., Viotti, M., and Hadjantonakis, A.K. (2008). The endoderm of the mouse embryo arises by dynamic widespread intercalation of embryonic and extraembryonic lineages. Dev. Cell *15*, 509–520.

Lanner, F., and Rossant, J. (2010). The role of FGF/Erk signaling in pluripotent cells. Development *137*, 3351–3360.

Lyashenko, N., Winter, M., Migliorini, D., Biechele, T., Moon, R.T., and Hartmann, C. (2011). Differential requirement for the dual functions of β-catenin in embryonic stem cell self-renewal and germ layer formation. Nat. Cell Biol. *13*, 753–761.

Marks, H., Kalkan, T., Menafra, R., Denissov, S., Jones, K., Hofemeister, H., Nichols, J., Kranz, A., Stewart, A.F., Smith, A., and Stunnenberg, H.G. (2012). The transcriptional and epigenomic foundations of ground state pluripotency. Cell *149*, 590–604.

Martin, G.R. (1981). Isolation of a pluripotent cell line from early mouse embryos cultured in medium conditioned by teratocarcinoma stem cells. Proc. Natl. Acad. Sci. USA *78*, 7634–7638.

Martinez Arias, A., Nichols, J., and Schröter, C. (2013). A molecular basis for developmental plasticity in early mammalian embryos. Development *140*, 3499–3510.

Najm, F.J., Chenoweth, J.G., Anderson, P.D., Nadeau, J.H., Redline, R.W., McKay, R.D., and Tesar, P.J. (2011). Isolation of epiblast stem cells from preimplantation mouse embryos. Cell Stem Cell *8*, 318–325.

Nichols, J., and Smith, A. (2009). Naive and primed pluripotent states. Cell Stem Cell *4*, 487–492.

Nichols, J., and Smith, A. (2011). The origin and identity of embryonic stem cells. Development *138*, 3–8.

Nichols, J., Silva, J., Roode, M., and Smith, A. (2009). Suppression of Erk signalling promotes ground state pluripotency in the mouse embryo. Development *136*, 3215–3222.

Niwa, H., Ogawa, K., Shimosato, D., and Adachi, K. (2009). A parallel circuit of LIF signalling pathways maintains pluripotency of mouse ES cells. Nature *460*, 118–122.

Ohnishi, Y., Huber, W., Tsumura, A., Kang, M., Xenopoulos, P., Kurimoto, K., Oleś, A.K., Araúzo-Bravo, M.J., Saitou, M., Hadjantonakis, A.K., and Hiiragi, T. (2014). Cell-to-cell expression variability followed by signal reinforcement progressively segregates early mouse lineages. Nat. Cell Biol. *16*, 27–37.

Osorno, R., and Chambers, I. (2011). Transcription factor heterogeneity and epiblast pluripotency. Philos. Trans. R. Soc. Lond. B Biol. Sci. *366*, 2230–2237.

Rossant, J. (2008). Stem cells and early lineage development. Cell *132*, 527–531.

Schrode, N., Saiz, N., Di Talia, S., and Hadjantonakis, A.K. (2014). GATA6 levels modulate primitive endoderm cell fate choice and timing in the mouse blastocyst. Dev. Cell *29*, 454–467.

Silva, J., and Smith, A. (2008). Capturing pluripotency. Cell *132*, 532–536.

Silva, J., Nichols, J., Theunissen, T.W., Guo, G., van Oosten, A.L., Barrandon, O., Wray, J., Yamanaka, S., Chambers, I., and Smith, A. (2009). Nanog is the gateway to the pluripotent ground state. Cell *138*, 722–737.

Smith, A. (2013). Nanog heterogeneity: tilting at windmills? Cell Stem Cell *13*, 6–7.

Spitz, F., and Furlong, E.E. (2012). Transcription factors: from enhancer binding to developmental control. Nat. Rev. Genet. *13*, 613–626.

ten Berge, D., Kurek, D., Blauwkamp, T., Koole, W., Maas, A., Eroglu, E., Siu, R.K., and Nusse, R. (2011). Embryonic stem cells require Wnt proteins to prevent differentiation to epiblast stem cells. Nat. Cell Biol. *13*, 1070–1075.

Tesar, P.J., Chenoweth, J.G., Brook, F.A., Davies, T.J., Evans, E.P., Mack, D.L., Gardner, R.L., and McKay, R.D. (2007). New cell lines from mouse epiblast share defining features with human embryonic stem cells. Nature *448*, 196–199.

Torres-Padilla, M.E., and Chambers, I. (2014). Transcription factor heterogeneity in pluripotent stem cells: a stochastic advantage. Development *141*, 2173–2181.

Toyooka, Y., Shimosato, D., Murakami, K., Takahashi, K., and Niwa, H. (2008). Identification and characterization of subpopulations in undifferentiated ES cell culture. Development *135*, 909–918.

Yang, S.H., Kalkan, T., Morissroe, C., Marks, H., Stunnenberg, H., Smith, A., and Sharrocks, A.D. (2014). Otx2 and Oct4 drive early enhancer activation during embryonic stem cell transition from naive pluripotency. Cell Rep. *7*, 1968–1981.

Ying, Q.L., Wray, J., Nichols, J., Batlle-Morera, L., Doble, B., Woodgett, J., Cohen, P., and Smith, A. (2008). The ground state of embryonic stem cell self-renewal. Nature *453*, 519–523.

Zhang, K., Li, L., Huang, C., Shen, C., Tan, F., Xia, C., Liu, P., Rossant, J., and Jing, N. (2010). Distinct functions of BMP4 during different stages of mouse ES cell neural commitment. Development *137*, 2095–2105.